Correspondence to:

C. M. Hall,
cmhall@umich.edu

Anomalous Noble Gas Solubility in Liquid Cloud Water: Possible Implications for Noble Gas Temperatures and Cloud Physics

Chris M. Hall[1] , M. Clara Castro[1] , Martha A. Scholl[2] , Julien Amalberti[3], and Stephen B. Gingerich[4]

[1]Department of Earth and Environmental Sciences, University of Michigan, Ann Arbor, MI, USA, [2]U.S. Geological Survey, Earth System Processes Division, Reston, VA, USA, [3]Institut für Geowissenschaften, Universität Potsdam, Potsdam, Germany, [4]U.S. Geological Survey, Oregon Water Science Center, Portland, OR, USA

Abstract The noble gas temperature climate proxy is an established tool that has previously been applied to determine the source of groundwater recharge, however, unanswered questions remain. In fractured media (e.g., volcanic islands) recharge can be so rapid that groundwater is significantly depleted in heavy noble gases, indicating that the water has retained noble gas concentrations from higher elevations. Previous studies of rain samples have confirmed a match to patterns seen in fractured-rock groundwater for heavy noble gases along with a significant helium excess. Snow has been shown to be a credible source for both the helium excess and the observed heavy noble gas pattern. Here, liquid cloud water samples were collected at two mountainous sites and analyzed for noble gas concentrations. A pattern like that of rainwater was found. However, an analysis of diffusive uptake of noble gases into cloud water demonstrates that droplets of 1 mm diameter and smaller should be in constant solubility equilibrium with the atmosphere. To explain this, we present a novel hypothesis that relies on the assumption that liquid water consists of two types of water molecule clusters bounded by hydrogen bonds: a low-density ice-like structure and a high-density condensed structure. In this model, the pressure gradient near the surface of a droplet resulting from surface tension could allow for the formation of a surface layer that is rich in ice-like low density clusters. This can explain both the helium excess and the heavy noble gas depletion seen in the samples.

Plain Language Summary Highly anomalous solubility values for atmospheric noble gases in small water droplets within clouds were found for samples from Puerto Rico and Virginia, USA. Various possible mechanisms were examined to explain the pattern of helium excess along with highly depleted argon, krypton, and xenon. A hypothesis is presented that assumes that an ice-like coating forms on micron-scale droplets due to the presence of large pressure gradients near the surface of small water droplets. It is assumed that these gradients can separate high density water molecule clusters from low density (ice-like) clusters because of buoyancy forces near the surface of the droplets. If confirmed by further research, this hypothesis has implications for the physics of cloud formation.

1. Introduction

The groundwater noble gas temperature (NGT) proxy has been used for nearly four decades (Aeschbach-Hertig et al., 2000; Ballentine and Hall, 1999; Hall et al., 2012; Kipfer et al., 2002; Mazor, 1972; Stute et al., 1992; Stute & Schlosser, 1993; Sun et al., 2010) as a paleoclimate proxy. It does not rely on calibration as do many other paleotemperature proxies because it utilizes the known temperature dependence of the water solubility of the four heaviest stable noble gases (Ne, Ar, Kr, and Xe). The temperature dependence of noble gas solubility in water increases substantially with increasing atomic mass (Ozima & Podosek, 2002). In practice, the concentrations of the atmospheric component of the heavier stable noble gases in groundwater are assumed to be a function of conditions existing at the water table at the time of recharge, which include both temperature and the altitude of recharge. With higher recharge altitude, the partial pressures of noble gases decrease, leading to lower dissolved concentrations in groundwater.

The solubility-controlled air saturated water (ASW) component of groundwater noble gas concentrations is conservative and dispersion of this component within an aquifer is a very slow process (e.g., Castro et al., 2007; Stute & Schlosser, 1993), and therefore groundwater is expected to record the temperature and pressure of the air

within the unsaturated zone at the time of recharge. Normally, this temperature is assumed to represent a close approximation to the mean annual air temperature (MAAT) at the location of recharge to the aquifer (see, e.g., Aeschbach-Hertig et al., 2000; Ballentine and Hall, 1999; Stute & Schlosser, 1993).

Noble gas concentrations in groundwater, especially those of the lighter noble gases, often exceed levels expected for ASW. Heaton and Vogel (1981) attributed these anomalously high noble gas concentrations to the incorporation and dissolution of air bubbles associated with rapid water table level changes. This excess air (EA) component is not a direct measure of temperature, as it reflects the air composition in entrained bubbles that are incorporated within groundwater. At deeper levels below the water table, the increased hydraulic pressure can force the dissolution of all noble gases. The EA component is richer in the light gases, especially Ne, than is the ASW component and the simplest NGT model, often referred to as the unfractionated air (UA) model assumes that the EA component consists of noble gases whose relative concentrations match those of standard air (Stute & Schlosser, 1993). Other more sophisticated EA models have been proposed; see Sun et al., (2010) for a review of a variety of proposed models and their statistical properties.

For typical sedimentary aquifers, where groundwater slowly percolates down to the water table in the recharge area, the NGT paleoclimate proxy is relatively well understood. However, in the case of areas with extremely rapid recharge, such as with aquifers that consist of fractured rock (e.g., basalt aquifers, karst), the acquisition of dissolved noble gases in groundwater is considerably more complex. Warrier et al. (2012) found that groundwater in the Galapagos islands was often deficient in the heavy noble gases by an amount that indicated that the water had not equilibrated with air at any possible recharge altitude for the islands. In addition, all samples displayed atmospheric He excesses. It appeared that, in effect, when recharge was very rapid, groundwater sometimes recorded precipitation signatures well above the altitude of an aquifer's recharge zone. A complete understanding of the mechanisms of the dissolution of noble gases in both precipitation and highly fractured media is vital if the NGT method is to be successfully used in the important role of determining the recharge zones for volcanic islands, which frequently have poorly understood hydrological systems (Niu et al., 2017, 2020; Warrier et al., 2012).

Prior to the Warrier et al. (2012) study, only a few measurements of noble gas concentrations in rainwater had been performed (Mazor, 1972). Subsequently, rainwater in SE Michigan was measured for noble gas concentrations and a recurring pattern emerged (Warrier et al., 2013). Rainwater was typically enriched in He and depleted in Ar, Kr, and Xe relative to the sampling conditions of temperature and altitude, with Xe being the most depleted and Ar the least. It was hypothesized that this pattern could be due to rainwater representing partially equilibrated ice, as Top et al. (1988) and later Malone et al. (2010) had found that He is more soluble in ice than in liquid water, with Ar, Kr, and Xe having extremely low solubilities. This argument could apply for sites like SE Michigan, where rain samples from mesoscale or larger storms were expected to have spent time in a frozen state due to high altitude even during summer. A further test of the hypothesis was done by Amalberti et al., (2018) where noble gases in fresh snow were measured, confirming that even fine-grained ice particles are enriched in He while being highly depleted in Ar, Kr, and Xe. Amalberti et al. (2018) argued that ice structure has a sufficiently large spacing to barely accommodate Ne and easily accommodate He. This space is too small, however, for the three heaviest stable noble gases. For detailed controls on noble gas concentrations in ice, see Utting et al. (2016) and Amalberti et al. (2018).

Additional tests of NGT systematics in fractured media were conducted on the island of Maui, Hawaii (Niu et al., 2017, 2020). Despite the fact that most of the recharge on the windward side of Maui was from rain and/or cloud water from low altitude clouds that never fall below the freezing point of water (Scholl et al., 2002), many of the same noble gas patterns were found in spring water samples as had been seen previously in Galapagos Island groundwater and SE Michigan rainwater samples. Specifically, the atmospheric component of He was in excess while the three heaviest noble gases were significantly depleted. In the case of Maui, it seemed implausible that ice or snow formation could be the cause of this unusual pattern of noble gas concentrations. Thus, we attempted to measure noble gas concentrations in liquid cloud water samples directly, to see if some of the patterns seen previously in fractured media aquifers were a direct result of recharge from small diameter water droplets within clouds. Indeed, cloud water is believed to account for a significant proportion of streamflow occurring on windward Maui (Scholl et al., 2002).

For the present study, liquid cloud water samples were collected to determine their noble gas concentrations. These measured values are compared to the expected concentrations given known noble gas solubilities and

diffusion coefficients. There is a substantial variance between the measured values and concentrations that were expected under the assumption that cloud water droplets are homogeneous liquid water in thermal equilibrium with air. Several alternative hypotheses are explored to account for the discrepancy between theory and empirical data and a mechanism is proposed that can account for many of the features observed in the data. For noble gases, cloud water droplets appear to act as if they are coated with a semi-permeable membrane that is structurally similar to water ice. If confirmed, this might have implications for other nonpolar hydrophobic species that can dissolve within clouds, along with theories connected to cloud condensation nuclei (CCN).

2. Sampling and Analytical Techniques

2.1. Cloud Water Sampling

Fog is small droplets of water suspended in the atmosphere, observed near or in contact with the land surface. It can be found in numerous settings, for example, overnight fog formed in valleys where temperature is below dew point, as coastal fog formed over the ocean and moving onto land, or as clouds formed in the atmosphere intersecting mountain slopes. Fog and cloud water research includes transportation hazards (Gultepe et al., 2007), fog as a human health hazard when it scavenges and alters the chemistry of atmospheric pollutants (Ervens et al., 2018; Pye et al., 2020), and fog or cloud water as a source of water and nutrients in ecohydrology (Weathers et al., 2006).

This study describes results from cloud water samples collected at two mountain sites that are frequently immersed in clouds. The two mountain locations have distinctly different climates and were chosen to observe the effects of different temperatures and moisture regimes on noble gases in cloud water. The mountain top site of Pico del Este is at 1,030 m within the Luquillo Experimental Forest (also El Yunque National Forest), Puerto Rico, a coastal tropical rainforest (designated herein as PR site, Figure 1). The slopes surrounding the site host a cloud forest ecosystem immersed in clouds during overnight hours ≥85% of the time (Bassiouni et al., 2017). Hydrometeorology and chemistry of the cloud system have been studied extensively at the site (e.g., Eugster et al., 2006; Gioda et al., 2013).

The Compton Gap ridge-top site is at 749 m in a humid temperate hardwood forest in the Shenandoah National Park, Virginia (designated herein as SNP site, Figure 1). Fog is common on the ridges and in valleys of the Appalachian Mountains and plays a role in the ecohydrology of the forests (Berry et al., 2014; Weathers et al., 2006). Samples were collected during periods when clouds were impacting the site and droplet density was sufficient to collect enough water for noble gas analysis.

A modified single stage Caltech Active Strand Cloudwater Collector (mini-CASCC, see Figure 2) was used to collect the cloud water samples (Daube et al., 1987; Demoz et al., 1996). The mini-CASCC is an active collector that is capable of extracting ~40–50 mL of water per hour from dense fog. A fan draws air through a polycarbonate box that has a series of six rows of PTFE monofilament. These collect water by droplet collision, and they are angled at 35° to the vertical to promote, via both gravity and aerodynamic drag, the rapid transport of water into a collection trough.

Clear plastic tubing was attached from the collection trough to the bottom of a refrigeration grade 3/8″ diameter copper tube for the purposes of collecting water for noble gas analysis. The collected cloud water was routed from the bottom so that the copper tube filled while avoiding the likelihood of entrapping air bubbles. The copper tube was held in a clamp device to make both an airtight and watertight seal (Weiss, 1968). For this study, each sampler was equipped with three stainless steel clamps so that two separate water samples of approximate volume of 6.5 mL were obtained during a single sampling period. See Figure 2 for a photograph of the sample collection equipment. Details of the conditions at the PR and SNP sites at the time of sampling are given in Table 1. It should be noted that the expected ASW concentrations for all the noble gases are extremely low compared to many other possible molecules in solution. For the sample with the highest ASW concentrations (SNP 18 November 2015, 12 pm), the expected concentrations as a mass fraction are 0.077, 0.17, 675, 0.34, and 0.079 ppb for He, Ne, Ar, Kr, and Xe, respectively. Thus, even for the highest concentration noble gas (i.e., Ar), all the gases can be considered as trace constituents of cloud water.
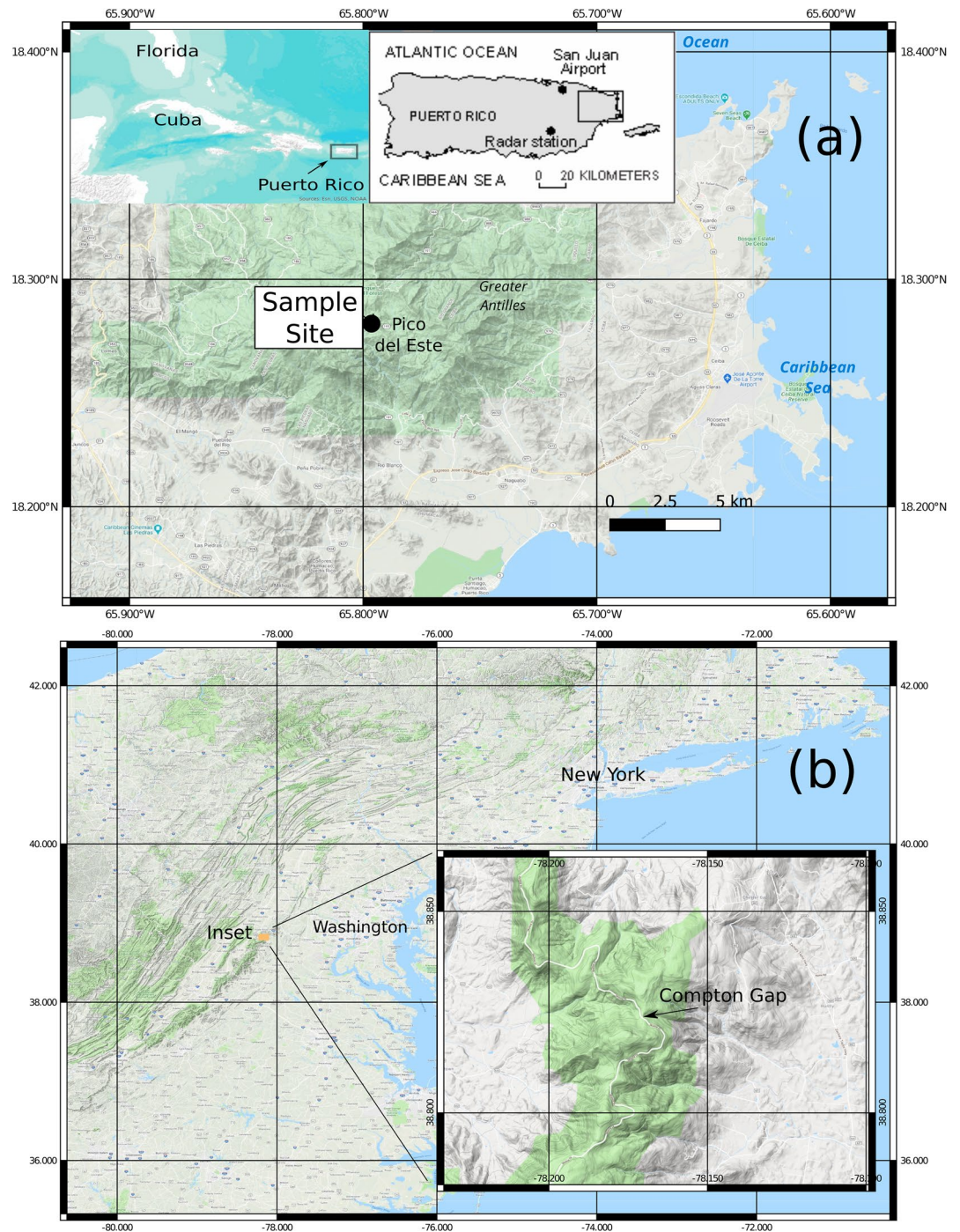
Figure 1. Sample site locations. (a) Pico del Este, Puerto Rico. (b) Compton Gap within the Shenandoah National Park.

2.2. Noble Gas Analysis

Water samples were analyzed for their noble gas composition at the Noble Gas Laboratory of the University of Michigan. Noble gas separation procedures were generally similar to those used in our earlier groundwater studies (e.g., Hall et al., 2012; Warrier et al., 2012); however, the subsequent installation of a new cryogenic separator system and two new mass spectrometers has led to significant detailed differences in the experiment methods.

Figure 2. Battery powered fog collector set up at Pico del Este, Puerto Rico. Upper inset shows the basic geometry of the collector, where cloud water droplets impinge on PTFE coated strings. Water drops then slide down the strings to a collection basin, and thence down a plastic tube to the bottom of a copper tube equipped with stainless steel pinch-off clamps. Filling the copper tube from the bottom reduces the chances of incorporating air bubbles.

Copper tubes were vertically attached to a vacuum extraction line and pumped down to a vacuum of ca. 1×10^{-5} Torr. Once a sufficient vacuum had been achieved, the sample was isolated from its turbo-molecular pump and its lower steel sealing clamp was removed. The copper tube was then squeezed to allow for the water to drain into a low-diffusion glass flask equipped with a magnetic stirrer to promote the release of dissolved gases. After stirring for 20 min, the sample section of the system was opened to a cold trap that was cooled by liquid nitrogen via a short length of small diameter tubing (1/16″ inside diameter stainless steel) for 10 min. The water vapor in the sample region acted as a carrier gas that pumped all dissolved gases into the cold trap. After closing the inlet valve to the cold trap, the trap was warmed to room temperature, thereby melting the small amount of water collected in the trap (~10–20 mL). The water vapor from the trap was then used to act as a carrier gas to pump noble gases for 15 s into a clean-up section using a tube filled with 3 Å molecular sieve, that traps water but not noble gases.

Once within the initial clean-up region, active gases were removed using a Ti sponge getter operated at 600°C. During the initial sample release and cleanup, a dual chamber cryogenic separator system was cooled down to an initial set of operating temperatures, with the high temperature chamber at 94°K and the low temperature chamber at ~20°K. The high temperature side of the cryo-separator bench is equipped with a Ti sponge getter operated at 600°C that is used for additional active gas clean-up and the low-temperature side of the bench has a room temperature Ti sponge getter that was used to reduce the H_2 partial pressure during the analysis of the ^{3}He/^{4}He ratio. Why is there extra vertical spacing here?

Both chambers are equipped with activated charcoal chambers, which mean that the low-temperature chamber can quantitatively trap all noble gases, including He. The three heaviest noble gases (Ar, Kr, Xe) were trapped at 94°K in the high-temperature chamber, after which He and Ne were trapped in the low temperature chamber at ~20°K. The release temperatures used were 49, 84, 210, 280, and 320°K for He, Ne, Ar, Kr, and Xe, respectively.

When the first sample was analyzed (PR 3/24/15 a), our Thermo Fisher Argus VI mass spectrometer was not yet operational, and all gases had to be

Table 1
Sampling Conditions

Pico del Este, Puerto Rico			Altitude = 1030 m		Location 18°16'08.3"N 65°45'31.0"W		
Date	Time	Average T (C)	ASW He	ASW Ne	ASW Ar	ASW Kr	ASW Xe
			ccSTP/g	ccSTP/g	ccSTP/g	ccSTP/g	ccSTP/g
24 March 2015	10:11	18.4	3.98E−08	1.65E−07	2.84E−04	6.41E−08	8.86E−09
26 March 2015	09:30	17.9	3.98E−08	1.66E−07	2.87E−04	6.49E−08	9.00E−09
27 March 2015	09:38	18.1	3.98E−08	1.66E−07	2.86E−04	6.46E−08	8.94E−09
18 August 2015	10:30	20.3	3.95E−08	1.63E−07	2.73E−04	6.11E−08	8.36E−09
17 September 2015	10:50	21.1	3.94E−08	1.62E−07	2.69E−04	5.99E−08	8.16E−09
Shenandoah National Park			**Altitude = 749m**		**Location 38°49'27.1"N 78°10'14.0"W**		
Date	Time	Average T (C)	ASW He	ASW Ne	ASW Ar	ASW Kr	ASW Xe
			ccSTP/g	ccSTP/g	ccSTP/g	ccSTP/g	ccSTP/g
18 November 2015	12:00	7.0	4.31E−08	1.90E−07	3.79E−04	9.10E−08	1.35E−08
18 November 2015	13:00	8.0	4.29E−08	1.88E−07	3.70E−04	8.83E−08	1.30E−08

Table 2
Normalized Noble Gas Concentrations (C/C$_{ASW}$) C$_{ASW}$ Values Calculated Based on Solubility Data Referenced in Ballentine and Hall (1999)

| Sample	He	Ne	Ar	Kr	Xe
1 sigma error (%)	1.5	1.3	1.3	1.5	2.2
PR 24 March 2015 a	1.15 E+00	1.08 E+00	9.01E−01	6.80E−01	5.36E−01
PR 26 March 2015 a	1.06 E+00	8.97E−01	7.17E−01	6.49E−01	5.65E−01
PR 26 March 2015b	1.04 E+00	8.89E−01	7.17E−01	6.17E−01	5.48E−01
PR 27 March 2015 a	1.09 E+00	1.02 E+00	9.27E−01	5.41E−01	3.30E−01
PR 27 March 2015 b	1.01 E+00	8.06E−01	5.98E−01	5.06E−01	4.46E−01
PR 18 August 2015-1 a	1.05 E+00	9.28E−01	7.38E−01	6.57E−01	5.82E−01
PR 18 August 2015-1 b	1.10 E+00	9.79E−01	8.06E−01	6.70E−01	6.04E−01
PR 18 August 2015-2a	1.10 E+00	1.07 E+00	9.92E−01	8.93E−01	6.07E−01
PR 18 August 2015-2 b	1.05 E+00	9.38E−01	7.66E−01	7.02E−01	6.54E−01
PR 17 September 2015-1 a	1.07 E+00	8.86E−01	6.94E−01	5.98E−01	5.25E−01
PR 17 September 2015-2 a	1.06 E+00	8.87E−01	7.31E−01	6.44E−01	6.09E−01
PR 17 September 2015-2 b	1.08 E+00	9.39E−01	7.80E−01	6.86E−01	6.36E−01
SNP 18 November 2015-1 a	1.05 E+00	9.43E−01	7.83E−01	7.57E−01	6.17E−01
SNP 18 November 2015-1 b	1.08 E+00	1.00 E+00	8.33E−01	7.96E−01	6.27E−01
SNP 18 November 2015-2 a	1.07 E+00	9.75E−01	8.37E−01	7.99E−01	6.62E−01
SNP 18 November 2015-2 b	1.05 E+00	9.54E−01	8.62E−01	8.66E−01	7.50E−01
Average C/CASW	1.07 E+00	9.50E−01	7.93E−01	6.91E−01	5.81E−01
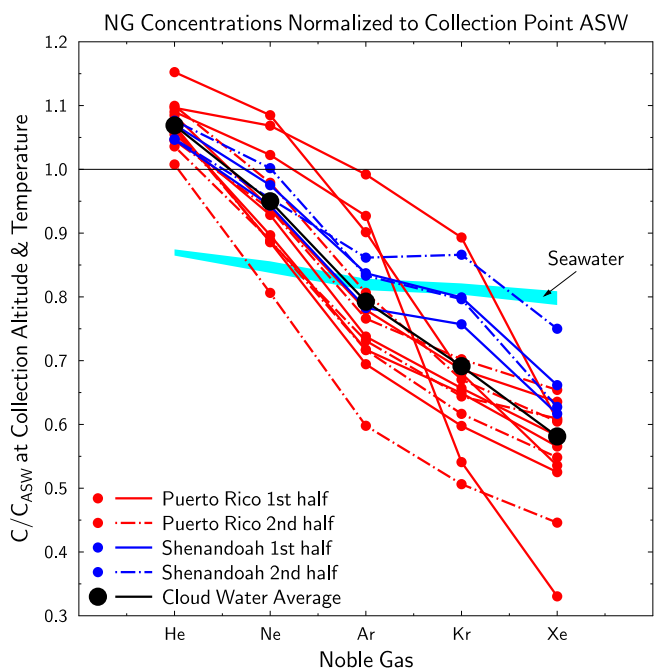
Figure 3. Noble gas concentrations to the ASW values expected at the temperature and altitude at the sample collection point. First and second half samples from a single copper tube are plotted separately. Shaded region in cyan represents the expected effect of dissolved solids with a NaCl molarity of 0.54 (approximate seawater composition) from a temperature of 7°C–20°C.

analyzed with a Thermo Fisher Helix SFT. Subsequently, all further samples' three heaviest noble gases (Ar, Kr, Xe) were analyzed using a Thermo Fisher Argus VI mass spectrometer. The Argus VI has significantly better performance for the measurements of isotope ratios for the three heaviest noble gases as it is possible to analyze multiple isotopes simultaneously. All isotopes were measured using Faraday detectors, except for ^{3}He, which was measured using an electron multiplier operated in ion counting mode. The Faraday preamplifier of the Helix SFT was operated with a feedback resistance of 10^{11} Ω. The Argus VI used 4 detectors with feedback resistances of 10^{12} Ω and one detector (High2) with a resistance of 10^{11} Ω. For Ar, all three isotopes (36, 38, and 40) were measured simultaneously. For Kr and Xe, series of two or three isotopes could be measured simultaneously. Both mass spectrometers were operated at a source ion trap current of 200 µA.

During the analysis campaign, there were frequent analyses of a known volume of outside air, which was used to calibrate both mass spectrometer ion source sensitivity and mass discrimination effects. Water samples that were equilibrated with air at a controlled temperature and 100% relative humidity were analyzed to verify that expected ASW concentrations could be measured with the above analytical technique.

3. Results

The results of the noble gas measurements are shown in Table 2 in the form of concentrations that are normalized to the expected air saturated water values (i.e., C/C_{ASW}) at the altitudes and temperatures existing at the time and location of sampling. These results are shown graphically in Figure 3, which

has a reference line at $C/C_{ASW} = 1$, which is the expected value if the cloud water had been in solubility equilibrium with air at the time of sampling. Detailed noble gas concentrations along with all measured isotopic ratios are provided in Table S1 in Supporting Information S1.

3.1. Noble Gas Concentrations

Normalized He concentrations ranged from 1.01 to 1.15 with a mean of 1.07, and SD of 0.033. Given the high diffusion coefficient of He at all the sampling temperatures, it is remarkable that all the samples yielded a small but significant He concentration excess. Ne concentrations ranged from 0.81 to 1.08 with a mean of 0.95 and SD of 0.072. In contrast to He, Ne was nearly in solubility equilibrium with water when sampled. For Ar, there were distinct indications of significant depletion below ASW values, with a range of 0.60–0.93, mean of 0.79 and SD of 0.098. This trend continued for Kr, with a range of 0.51–0.89, a mean 0.69 and SD of 0.108. Finally, Xe had a range of 0.33–0.75, a mean of 0.58 and SD of 0.095.

An interesting pattern is apparent for the Shenandoah samples, where Kr concentrations did not drop off as quickly from Ar concentrations as they did for the Puerto Rico samples. In addition, the Kr and Xe concentrations for the Shenandoah samples were, on average, slightly closer to solubility equilibrium than were the Puerto Rico samples. There is an almost linear trend in the average decline of the measured C/C_{ASW} values if one regards He as noble gas #1 and Xe is noble gas #5; however, there is considerable variability between both individual samples and between runs of the two separate halves of a single sample tube, referred to as "first half" and "second half" in Figure 3.

For PR samples 3/24/15 and 9/17/15-1, the internal steel clamp on the Cu sampling tube did not seal sufficiently to allow for the analysis of a "b" half. It is clear from the data in Table 2 that results from the "a" and "b" halves of a Cu tube, when available, are more distinct than expected from the precision estimates alone. This indicates that the water that flowed into the tube was not completely mixed, that the two halves of a tube are not, strictly speaking, replicates, and that within the inside diameter of 0.25″ (6.35 mm), there was little internal mixing during sampling. This is compatible with the results from a continuous water sampling system used to monitor temporal variations of noble gases in Monterey Bay, CA, USA by Füri et al. (2009). Cloud water that collects in the sampler trough then flows into the sampling tube will tend to equilibrate with air, such that over time, each noble gas C/C_{ASW} should move toward the value of 1. The degree to which that happens will depend on the rate of sample collection and upon temperature. Temperature is a factor because the diffusion coefficients of the noble gases in water are temperature dependent, with higher diffusion rates expected for higher temperatures. The differences between "a" and "b" values for Puerto Rico samples average 5.5%, 9.2%, 13.5%, 6.3%, and 4.6% for He, Ne, Ar, Kr, and Xe, respectively. The equivalent values for Shenandoah samples are 2.6%, 4.0%, 3.8%, 5.3%, and 5.0%. Using the diffusion coefficient Arrhenius constants from Ballentine and Hall (1999) and assuming an average sampling temperature of 19.5°C for Puerto Rico samples and 7.5°C for Shenandoah, noble gases should have diffused into Puerto Rico samples faster than Shenandoah samples by factors of 23%, 30%, 44%, 43%, and 46% for He, Ne, Ar, Kr, and Xe, respectively.

For both sets of samples, the differences are relatively low for He, as this gas is not only, on average, close to being in equilibrium, it is also the one with the highest diffusion coefficients. It is interesting to note that there is much more consistency between results for the "a" and "b" results for the Shenandoah samples than for the Puerto Rico samples. Since the Shenandoah samples were collected at a lower temperature than those from Puerto Rico, this is consistent with the idea that diffusion rates might have exerted at least partial control over the differences seen within a single Cu tube.

3.2. Isotope Fractionation

Representative isotopic ratios for four of the sampled noble gases are displayed in Figure 4 along with mass-dependent fractionation (MDF) lines, which are the pattern for fractionation expected from diffusive transport. Most Ne values shown in Figure 4a are close to the MDF line, with the majority of both Puerto Rico and Shenandoah samples being rich in the light isotopes (i.e., above and to the right of the air value). The points that plot below and to the left (i.e., rich in heavy isotopes) are likely less reliable because they have unusually large scatter in the raw data. The Helix SFT sector magnet is large, with significant field heterogeneities, which can cause inconsistent data collection if extra peak centering is not performed frequently during data collection. Since these
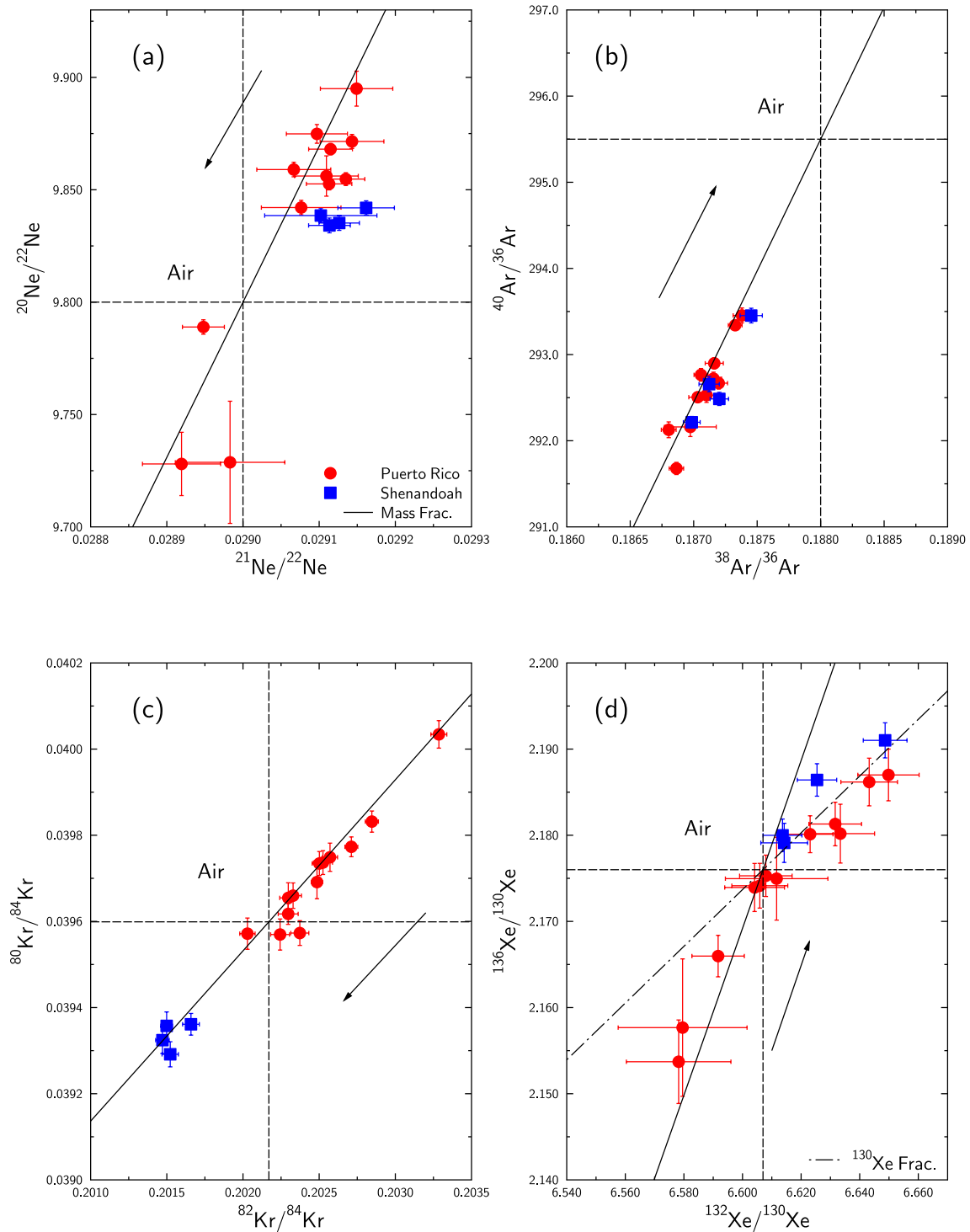
Figure 4. Measured isotope ratios. (a) $^{20}Ne/^{22}Ne$ versus $^{21}Ne/^{22}Ne$. (b) $^{40}Ar/^{36}Ar$ versus $^{38}Ar/^{36}Ar$. (c) $^{80}Kr/^{84}Kr$ versus $^{82}Kr/^{84}Kr$. (d) $^{136}Xe/^{130}Xe$ versus $^{132}Xe/^{130}Xe$. Dashed lines indicate air values. Solid line indicates a mass dependent fractionation line (MDF) trend. Arrows show the direction along the MDF line that is enriched in heavier isotopes. Most points fall close to the MDF trend, except for some Xe ratios to the right of the line. These may be due to mass independent fractionation of ^{130}Xe relative to ^{132}Xe and ^{136}Xe.

samples were measured, additional precautions have been implemented, but for this data set, we consider the Ne isotope ratios to be the least reliable ones measured.

The Ar isotopes plotted in Figure 4b show excellent concordance with the MDF line, with all samples from both sites displaying enrichment in the lighter isotopes. This is strong evidence that Ar in all of the cloud water samples is not in solubility equilibrium and that during sample collection, Ar was being transported into the water samples at a rate that was mass dependent (e.g., via diffusion). The isotopes of Kr plotted in Figure 4c also fall extremely close to an expected MDF line. For Kr, because the heaviest isotope in the ratios, that is, ^{84}Kr, is in the denominator, samples rich in heavy isotopes plot below and to the left of air and samples rich in light isotopes plot above and to the right of air. The pattern is distinctly different from that for Ar, as Shenandoah samples are all rich in heavy isotopes while Puerto Rico samples vary from being nearly unfractionated to being significantly enriched in light isotopes. The Puerto Rico samples are consistent with Kr diffusing into the water samples via a velocity mediated mechanism. However, even though all Shenandoah samples are depleted in Kr, their Kr compositions are rich in heavy isotopes. Under the sampling conditions for the Shenandoah samples, the mechanism that controls the solubility must favor heavier, slower-diffusing isotopes and this issue is discussed below.

For Xe, the situation appears to be more complicated. The isotope ratios plotted in Figure 4d show samples that range from being rich in light isotopes to those that are rich in heavy isotopes. However, several points deviate significantly from the MDF line and are more compatible with mass independent fractionation (MIF) of ^{130}Xe. This issue is explored more thoroughly in Section 3 and Figure S5 in Supporting Information S1. Briefly, there is evidence for MIF depletion of isotopes 128 and 130 relative to the three heaviest Xe isotopes. In addition, both isotopes 129 and 131 are enriched relative to isotope 130, suggesting a possible optical mechanism that uniquely affects odd numbered isotopes, as is seen for the isotopes of Hg (e.g., Bergquist & Blum, 2009). This complex pattern of MIF for Xe suggests that there is some feature on the surface of cloud water droplets that can slightly modulate the solubility of individual Xe isotopes.

It should be noted that the degrees of isotope fractionation seen for Ar, Kr, and Xe are significantly in excess to those found by Seltzer et al. (2019). In that study, the effects of diffusive transport and isotope-dependent solubility were measured with a precision of <0.1‰. Solubility differences cannot explain the fractionation shown in Figure 4. Diffusion effects are certainly possible for the water samples equilibrating with air after collection within the fog collector, but it would not be expected within liquid cloud particles since they should be in solubility equilibrium (Seinfeld & Pandis, 2016, ch. 11). An analysis of the maximum time for falling water droplets to be out of noble gas solubility is presented below.

4. Discussion

To assess the implications from the results shown above, we must examine what would be expected given the known solubilities for the noble gases in water, along with likely transport mechanisms. The results show a consistent pattern of He enrichment along with considerable depletion in Ar, Kr, and Xe. Ice and snow are extremely depleted in the heavy noble gases (Amalberti et al., 2018; Malone et al., 2010; Top et al., 1988; Utting et al., 2016) and it is natural to examine how one would expect water droplets that form from melting snow or ice pellets to evolve in terms of their noble gas concentrations during the course of falling to the ground. The question is, would one expect rain or small-diameter cloud water droplets to retain any "memory" of an origin as ice and thereby present as water with He enrichment and heavy noble gas depletion? If so, what droplet sizes might have this pattern? In Section 4.1, we examine this question using a simplified water droplet model that assumes standard values of temperature dependent solubilities and diffusion coefficients in water.

In addition, are there any modifications to standard noble gas solubilities that can explain our results in cloud water? In Section 4.2, we examine the results of applying the NP model of Mercury et al. (2003, 2004) to the case of small water droplets with significant positive pressure caused by surface tension, that is, Young-Laplace pressure (De Gennes et al., 2013).

4.1. Model for Noble Gas Uptake From Melted Snow and Ice

In this simplified model, it is assumed that snow crystals or ice pellets that form at high altitude in a cloud melt at 0°C and continue falling as a spherical water droplet. The initial noble gas concentrations, normalized to ASW
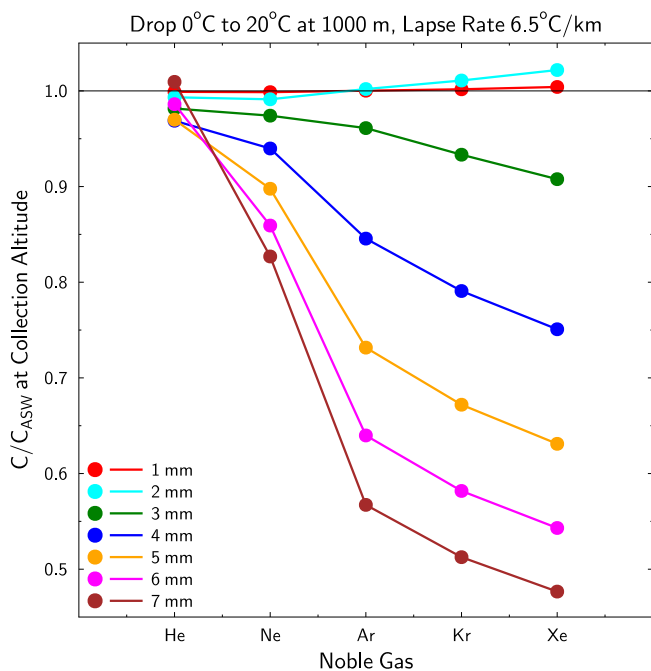
Figure 5. Modeled normalized noble gas concentrations (C/C$_{ASW}$) of droplets that start as melted ice at 0°C and fall to an altitude of 1000m with an assumed temperature of 20°C. The droplet is assumed to drop at terminal velocity determined by its diameter and the atmospheric pressure. Droplets are assumed to be in thermal equilibrium with the surrounding air. Initial C/C$_{ASW}$ values are assumed to be 2, 0.8, 0, 0, and 0 for He, Ne, Ar, Kr, and Xe, respectively. Boundary conditions are set by the pressure, temperature of the air as the droplet falls and the corresponding Henry's constants. All noble gas transport is assumed to be due to diffusion.

at the initial altitude and 0°C (i.e., C/C$_{ASW}$) are assumed to be 2, 0.8, 0, 0, and 0 for He, Ne, Ar, Kr, and Xe, respectively. These values were used for the ice modeling in Malone et al. (2010) and closely match values found in Amalberti et al. (2018).

The water droplet is assumed to fall at terminal velocity according to the simplified empirical relationship of Best (1950), which has the advantage over other formulae in that terminal velocity is guaranteed to be non-negative for all values of droplet diameter (e.g., see equations in Foote & Du Toit, 1969). Atmospheric pressure is assumed to follow a simple exponential relationship, as in Ballentine and Hall (1999). The modeling software can use an input lapse rate along with a collection point altitude and temperature to define a vertical temperature profile that the falling droplet encounters as it falls from a temperature of 0°C to the collection point.

The sole transport mechanism into the droplet is assumed to be via noble gas diffusion within the liquid water droplet. This is a very conservative assumption since any stirring or advection within the liquid water will enhance the uptake of noble gases. For example, in Elperin et al. (2009), it was assumed that the interior of a droplet has a uniform concentration beneath a thin diffusive boundary layer. Therefore, the model results presented here should be considered the absolute minimum change expected in the C/C$_{ASW}$ value for any noble gas to move from initial ice values toward a value of 1, that is, solubility equilibrium.

The boundary condition for the droplet is that the surface value of the concentration C should be the C$_{ASW}$ appropriate for the altitude and temperature at any moment during the droplet's fall. This value is determined by both pressure and the temperature dependent Henry's constant for each of the noble gases. Because the diffusion coefficients for all noble gases in air are much faster than those in liquid water (e.g., Huber et al., 2006; Jähne et al., 1987), the concentration of noble gases in air at the droplet surface is assumed to be the standard value for air at 100% relative humidity.

Due to the highly nonlinear nature of this problem, it has been solved numerically. The atmosphere is divided into 10,000 layers and analytical solutions at constant pressure and temperature are found using a Fourier series solution to the diffusion equation at each layer. Details of the underlying equations and the solution techniques used are given in Section 1 of Supporting Information S1.

A series of simulations were run for lapse rates of 6.5 and 4.7°C/km, which approximately covers the expected range for wet (moist adiabatic) lapse rates (e.g., Manning & Solomon, 2003; Niu et al., 2017; Niu et al., 2020; Wallace & Hobbs, 2006). The result of one such simulation is shown in Figure 5 for a lapse rate of 6.5°C/km. Plotted are expected values of C/C$_{ASW}$ for the noble gases at the collection altitude of 1,000 m a.s.l. and a collection temperature of 20°C for droplets ranging in diameter from 1 to 7 mm. Droplets larger than 3 mm in diameter would have fallen fast enough so that they retain a memory of their initial depletion in Ar, Kr, and Xe. However, only the largest droplets shown retain any of their initial He excess. At these temperatures, He diffusion is fast enough that one would expect all of the initial He excess to have been removed and droplets will have retained a signature of being at higher altitudes where the He partial pressure is lower than at the collection point. An interesting feature of the results shown in Figure 5 is that of the Xe value for a 2 mm diameter droplet. For raindrops of that size, the terminal velocity is slow enough so that Xe can partially equilibrate with the water at lower temperatures and since the solubility of Xe is very temperature sensitive, it is possible for water to acquire a slight Xe excess despite starting with a concentration of zero.

The results from further simulations are shown in Supporting Information S1 for collection point temperatures of 10°C and for a lapse rate of 4.7°C/km (Figures S1–S3 in Supporting Information S1). Features are very similar to those of Figure 5, however, for a collection point temperature of 10°C, the diffusion of He out of the water droplet
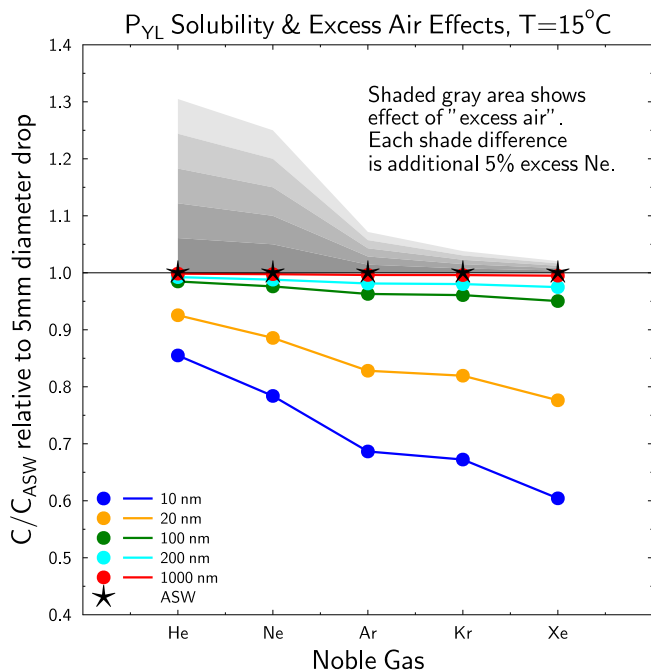
P$_{YL}$ Solubility & Excess Air Effects, T=15°C

Figure 6. Equilibrium solubility values for small droplets due to Young-Laplace pressure based on the thermodynamic model of Mercury et al. (2003). Solubility of all gases decreases due to surface tension induced positive pressure, but the effect is only significant for extremely small droplet diameters (<100 nm). Excess He can occur due to excess air (gray shaded regions), but this will also lead to excess Ne.

is sufficiently retarded that water droplets might be expected to retain at least some of their initial He excess. It must be noted, however, that for droplets of about 1 mm diameter, the terminal velocity is slow enough that one would expect such rain to be in nearly continuous equilibrium with the surrounding air and that one should not see a significant depletion in the concentrations of the three heaviest noble gases.

This point is further illustrated by the results of a simulation showing what might be expected for melted snow to only fall a distance of 1 m at a temperature of 0°C. In FIgure S4 in Supporting Information S1, we can see that droplets with a diameter of 100 μm or smaller should be in equilibrium for all noble gases after only falling 1 m, and this droplet size is significantly greater than the roughly 2–50 μm size range expected for cloud water in Puerto Rico and the Appalachian Mountains (Li & Aneja, 1992; Speigel et al., 2014). This strongly suggests that there is some mechanism that significantly alters the solubility of noble gases in liquid cloud water droplets.

4.2. Negative Pressure Model of Noble Gas Solubilities

From the above analysis, given the diffusivity of noble gases in water, liquid cloud water clearly should be in continuous equilibrium with respect to noble gas solubility at ambient pressure and temperature conditions. This suggests that there must be some other mechanism that greatly modifies the solubility of noble gases within small diameter water droplets.

One possibility that was examined was the negative pressure (NP model) solubility model proposed in Mercury et al., (2003, 2004). This solubility model was developed to help explain apparently high solubilities for heavy noble gases in groundwater. The NP model examined the thermodynamics of noble gas solubility in the presence of concave water surfaces due to capillary action at the air-water interface at the water table. In the case of cloud water droplets, there is a positive pressure difference between the interior of a droplet and the outside air pressure (Young-Laplace effect), which is given by:

$$P_{YL} = \frac{2\gamma}{a} \tag{1}$$

where γ is the surface tension of water and a is the droplet radius. As a reasonable approximation, the excess pressure will be equal to 1 atmosphere for a droplet with a diameter of about 3 μm. When one employs the analysis of Mercury et al. (2003, 2004) for the case of positive pressure, noble gas solubilities will decrease, with the effect being greatest for the heavy noble gases. This is precisely the effect that could conceivably explain the results shown in Figure 3.

Shown in Figure 6 are a series of calculated values of C/C$_{ASW}$ for droplets ranging in diameter from 10 to 1,000 nm. For diameters of 20 nm or less, there is a distinct reduction in solubility for the three heavy noble gases. However, the extremely small diameters needed to produce the high internal pressures required to create these effects are much smaller than the range of roughly 2–50 μm expected for suspended liquid cloud droplets at these sites. Although small diameter droplets could conceivably have coalesced to form larger droplets with diameters greater than 1 μm, the results of simulations shown in Figure 5 and Figure S1–S4 in Supporting Information S1 show that these droplets should immediately equilibrate with the atmosphere with respect to noble gas concentrations.

An additional problem with the Mercury et al. (2003, 2004) model to explain the measured cloud water solubilities is that elevated Young-Laplace pressure reduces solubility for all noble gases, including He. This is in contrast to the measurements illustrated in Figure 3, where almost all of the samples yielded excess He concentrations. Conceivably, excess He might have been caused by the presence of excess air resulting from air bubbles entrained in the plastic tubing and Cu sample tubes (Aeschbach-Hertig et al., 1999, 2000; Ballentine and Hall, 1999; Mazor, 1972; Stute & Schlosser, 1993, etc.). The effect of unfractionated air (UA model) is shown as varying

shades of gray in Figure 6. However, excess air would also increase concentrations of the heavier noble gases and it is unlikely that our cloud water results could be due to the serendipitous addition of just the right amount of excess air to cloud water whose heavy noble gas solubilities had been reduced via the Mercury et al. (2003, 2004) NP model, even if some unforeseen mechanism could have preserved these noble gas concentrations as droplets grew from roughly 10 nm diameter up to diameters of 2–50 μm.

One might also speculate that the cloud water droplets were coated with a film that effectively reduced heavy noble gas solubility while enhancing helium solubility. However, it seems unlikely that a contaminant could be the cause of this behavior for both sampled sites, as the flora, proximity to the ocean, temperature, and industrial pollution levels at Pico del Este in Puerto Rico are quite distinct from Shenandoah. We note that solubilities of noble gases in hydrocarbons are higher than those for liquid water.

In the next section, we explore the possibility that a film with the required noble gas solubility properties does in fact develop on the surfaces of cloud water droplets; however, the film is not a foreign substance, but liquid water itself.

4.3. Yet Another Anomalous Behavior of Water?

For well over a century, researchers have noted the many scores of anomalous properties displayed by water, both in its solid and liquid form (e.g., Ball, 2008). These include unusual heat capacity, surface tension, heat of fusion, viscosity, and temperature dependence of density. The latter property is why ice floats and why lakes that freeze over during winter overturn every spring. It has long been surmised that liquid water behaves as if it is a mixture of two separate liquids with differing structural properties. This polymorphism behavior, where water behaves as a combination of a high-density liquid phase (HDL) and a low-density liquid phase (LDL), although not universally accepted, does provide a framework for understanding many of the unusual properties of water. See Gallo et al. (2016) for a review of the subject.

Chaplin (2000) proposed that the LDL and HDL components of liquid water could be the result of the formation of clusters of water molecules that are bound together by hydrogen bonds, with *expanded* low density structures (ES) accounting for the LDL component and *condensed* high density structures (CS) the HDL component. This general approach has been pursued both experimentally and theoretically to the present time (e.g., Buck et al., 2014; Gallo et al., 2016; Garcia-Ratés et al., 2011; Müller et al., 2003).

Huang et al. (2013) noted that it was energetically favorable to have ES style clustering at a water surface, where water molecules have a reduced number of nearest neighbors. The proposed ES cluster structure in Chaplin (2000) is similar to that of ice and this is a promising possible line of evidence that could lead to a mechanism that would help to explain the anomalous solubility measured for our cloud water samples. However, just favoring ES clusters at the air-water interface alone does not explain our results, because water with a flat or nearly flat air water surface (i.e., no curvature) does not display anomalous solubility. Some feature of small diameter water droplets must promote the solubility of He and greatly diminish the solubility of Ar, Kr, and Xe.

From Equation 1, a significant excess pressure can develop within a cloud water droplet due to the surface tension of water. The interior of the droplet must be at a nearly uniform pressure as otherwise the interior liquid would flow toward the surface of the droplet. There must be a significant pressure gradient very near the surface, where near-surface water molecules are under significant tensile stress. Douillard (2009) reported that the air-water interface consists of a depletion layer with a thickness of ~0.5 nm. This was confirmed by Tarasevich (2011), who also noted that X-ray data suggest that liquid water has an unusually well-ordered structure up to a depth of ~35 nm below the air–water surface. Likely, any pressure gradient that might exist beneath the surface of a liquid cloud water droplet extends for no more than a depth of a few nm.

As noted in Section 2 of Supporting Information S1, if the effective water surface thickness is 2 nm, then for a droplet with a diameter of 3 μm, the pressure gradient near the surface would be equivalent to a centrifuge with an acceleration of 5 billion times that of gravity. If water has a very high pressure gradient, then buoyancy forces will push low density ES structures toward the lowest pressure zones (i.e., the surface of a droplet) and high density CS structures would tend to sink toward the high pressure interior of the droplet. This is illustrated as a cartoon in Figure 7.
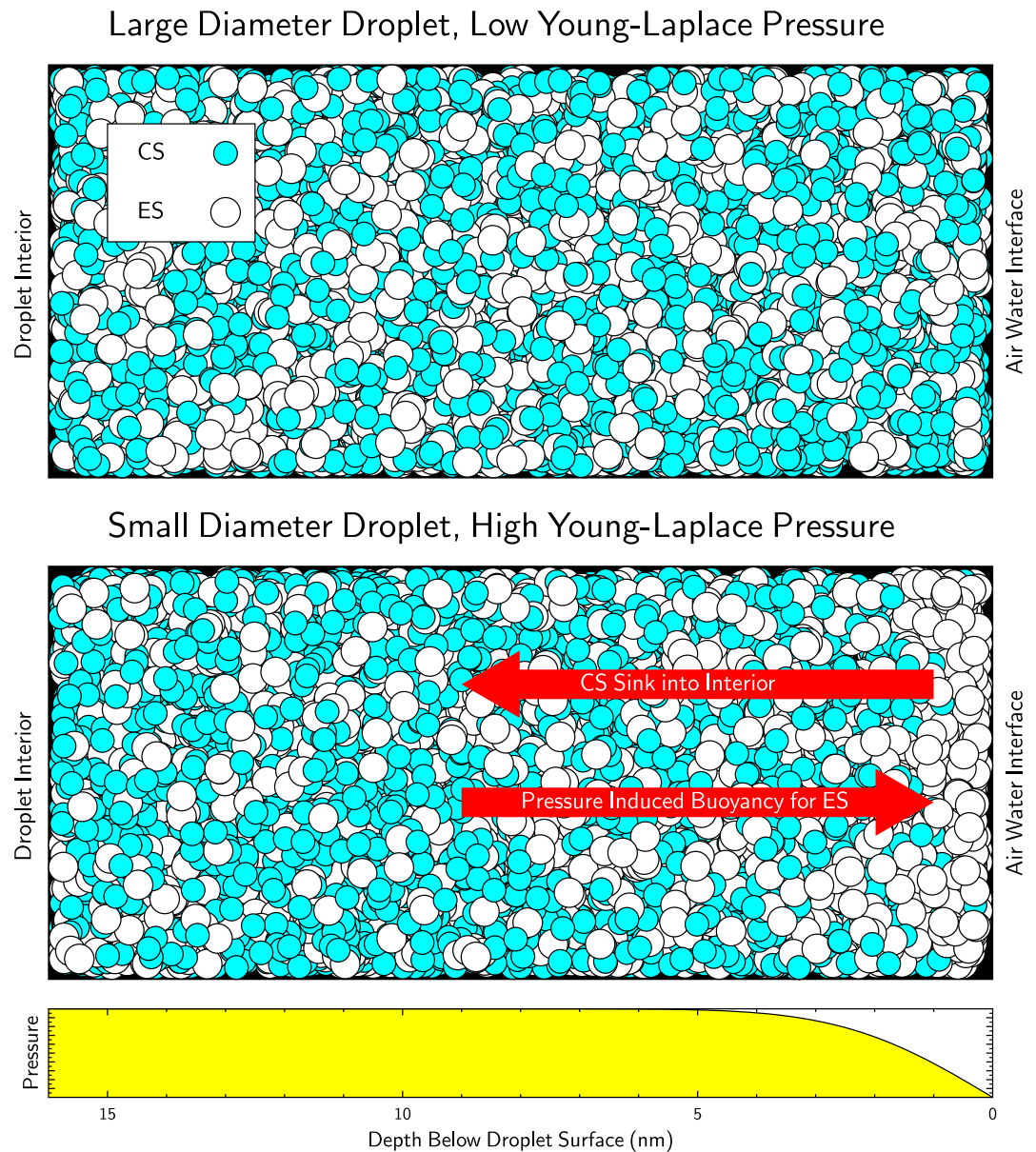
Large Diameter Droplet, Low Young-Laplace Pressure

Small Diameter Droplet, High Young-Laplace Pressure

Figure 7. Cartoon showing possible mechanism that could concentrate expanded structure (ES) clusters at the surface of a droplet due to buoyancy caused by a hit Young-Laplace pressure gradient. In addition, denser condensed structure (CS) clusters will tend to "sink" inward toward the droplet interior. Clusters not shown to scale. In the upper diagram, the cluster population at the surface is identical to the bulk water composition. For small diameter droplets with a high pressure gradient (middle diagram), the surface is dominated by a high concentration of ES clusters.

Equations S13–S15 give the force expected to be exerted on ES and CS structures under differing assumptions about the surrounding water density. Assuming the temperature dependent ES and CS density model of Veda-muthu et al. (1994) along with Stoke's Law, it is possible to calculate the sinking velocity expected for CS clusters that form at the surface of a droplet whose surface is populated solely by ES clusters. The results of these calculations for 40 and 280 molecule clusters are shown in Figure 8a. For a droplet with a diameter of ∼5 µm, one would expect a 280 molecule CS cluster at the surface to sink toward the interior with an initial velocity of about 2,000 µm/s, which means that it could traverse a surface layer with a thickness of 2 nm in roughly 1 µs. If ordered ES and CS clusters are long-lived on the time scale of micro-seconds, then this might be a possible mechanism for droplets to continually resurface themselves. Figure 8a also shows the average diffusion velocity expected at
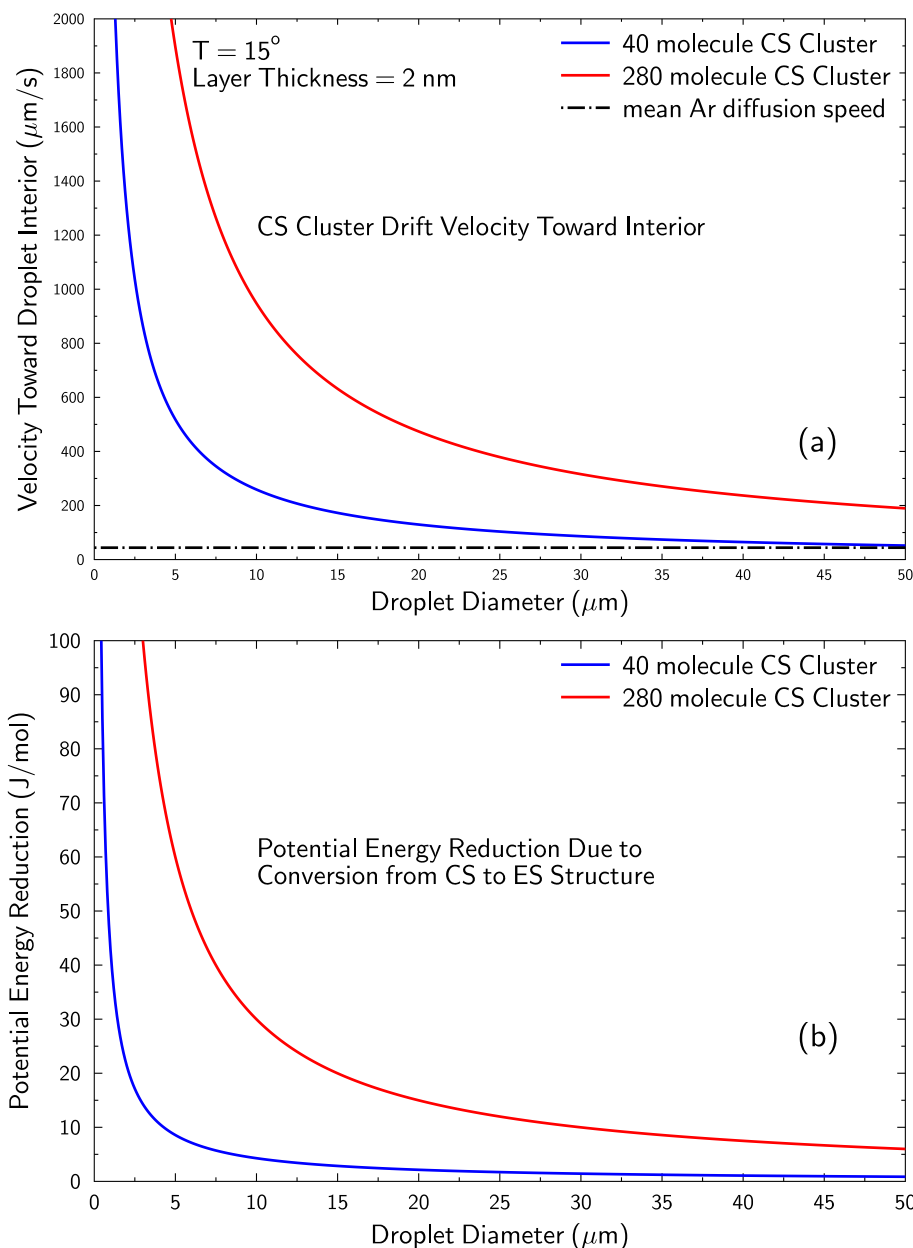
Figure 8. Possible properties of CS clusters at the surface of a droplet which consists entirely of ES clusters. (a) Expected drift velocity of 40 and 280 molecule clusters inward toward the droplet interior. Dashed line indicates the expected average random walk distance per second for an Ar atom. (b) Reduction of potential energy expected per mole of clusters for a CS cluster to rearrange into an ES cluster.

15°C for an Ar atom in liquid water and the CS cluster sinking velocity exceeds the diffusion speed of Ar over a broad range of cluster and droplet sizes.

On the other hand, if water clusters rapidly shift back and forth between ES and CS configurations on time scales much shorter than 1 μs, then a drift model that assumes that CS clusters on the surface of a droplet sink into the interior becomes less tenable. Instead, the potential energy cost of a CS cluster being on the surface of a droplet could be enough to bias cluster formation to the more ordered ES form. Thus, even if clusters might not migrate for significant distances, the dynamics of cluster formation could still produce the effect that we hypothesize. Mishima and Stanley (1998) argued that the LDL (ES cluster) form of water is the most stable form of water at room temperature, but that there is a slight local minimum of the total energy of formation that corresponds to

the HDL (CS cluster). The HDL form is favored at room temperature because the CS cluster structure has higher entropy than the more highly ordered ES structure. Chaplin (2000) noted that the energy difference between the two forms can be low, because no hydrogen bonds are broken if an ES cluster compresses to form a CS cluster. Using Equation S19 in Supporting Information S1, we show in Figure 8b the energy cost per mole of water clusters for CS clusters to reside on the surface of a droplet whose surface is dominated by ES clusters. If the energy cost is similar in size to the local energy minimum for a CS cluster in the absence of a pressure gradient, then one can see that small water droplets might favor ES clusters near the air-water interface.

By making some simplifying assumptions outlined in Supporting Information S1, it is possible to estimate the effective thickness of a surface layer that is rich in ES clusters. The Gibbs free energy of a droplet is assumed to be the same as a droplet with no pressure gradient (i.e., no surface tension). Enthalpy is reduced by the formation of the ES surface layer, but this comes at the cost of an entropy decrease caused by the confinement of CS clusters into the interior of the droplet below the surface layer. Where these two factors intersect is the point where there is no external work on the droplet and the thickness that satisfies this criterion is nearly independent of droplet diameter. As illustrated in Figure S5 in Supporting Information S1, the thickness of the surface layer should be about 2.7 nm for water clusters averaging about 40 molecules each. Although the surface thickness should be roughly constant with respect to droplet diameter, the reduction in enthalpy is highly dependent on the diameter, suggesting that the cohesiveness of any ES-rich surface layer should be greatest for the smallest droplets within a cloud (see Figure S5 in Supporting Information S1).

If a thin film that is rich in ES clusters does form on small diameter cloud water droplets, then our noble gas solubility data can be understood as being the result of a semi-permeable ice-like barrier that forms at the air-water interface. From previous studies (e.g., Amalberti et al., 2018), it is known that the relatively open structure of water ice accommodates He at roughly twice the solubility of liquid water and we expect that ES clusters being preferred at a droplet's surface could indeed increase the apparent solubility for He in cloud water. Ice and liquid water have similar Ne solubility, which is compatible with our cloud water data. Both He and Ne can likely be accommodated within the interior of ES water clusters.

Voids in the structure of ice are too small to easily incorporate significant quantities of the three heavy noble gases (Ar, Kr, and Xe). This can partially explain our noble gas solubility results, as all three heavy noble gases are depleted with respect to their expected liquid water concentrations. Ar is the least depleted and Xe is the most and this could partially be due to kinetic effects of partial equilibration within the fog collector after droplets coalesce and begin draining into the copper tube. However, it is also possible that this pattern of depletion of the heavy noble gases could be due to imperfections in the ES cluster film on a droplet surface. If the liquid water surface is a dynamic feature, with continually shifting boundaries between ES clusters, heavy noble gases can be partially accommodated. Surface defects can possibly be formed if a cluster briefly is compressed to the CS form and then either reform as an ES cluster or sinks inward toward the interior of the droplet.

The lightest of the three depleted gases (Ar) will also have the highest thermal velocity within air and could enter any imperfections most rapidly. In contrast, Xe is the slowest and could be expected to be less likely to enter via any surface film defects. Heavy noble gases cannot be accommodated within a cluster having the relatively open ES structure much less within the denser CS structure. This suggests that solubility of the heavy noble gases within liquid water is normally controlled by spaces between water molecule clusters as opposed to being contained within clusters. Holz et al. (1994) noted that the activation energy values for the diffusion of Ne and Xe in water was less than the activation energy for the self-diffusion of water. This could be compatible with the concept that noble gases reside between clusters of water molecules if self-diffusion of water requires the rearrangement of hydrogen bonds within clusters.

The isotopic fractionation patterns shown in Figure 4 may give some clues to the mechanism for noble gas solubility in cloud water. For both Puerto Rico and Shenandoah samples, Ar is very enriched in the light isotopes, which can be explained by an incorporation mechanism that is controlled by transport of Ar within the gas phase moving toward short-lived spaces between water molecule clusters on the droplet surface. For Kr, there is an interesting difference between Puerto Rico and Shenandoah samples. Puerto Rico samples range from being identical to air up to being enriched in light isotopes, but the Shenandoah samples are uniformly enriched in heavy isotopes. The Shenandoah samples were collected at a lower temperature than the Puerto Rico samples and at lower temperatures, the capture of Kr might possibly be enhanced by the presence of Kr atoms that have

adhered to the droplet surface. We note that the temperature for quantitative release of Kr from activated charcoal in our cryo-trap is nearly identical to the temperatures during Shenandoah sampling. For Xe, most samples from both Puerto Rico and Shenandoah are enriched in heavy isotopes, suggesting that surface adhesion may be an important factor for this noble gas. The issue of Xe fractionation is more complex than for the other heavy noble gases, as there appears to be both mass-dependent and mass-independent effects (Figure S7 in Supporting Information S1). This is discussed in more detail in Section 3 of Supporting Information S1.

4.4. Possible Implications for Noble Gas Temperatures and Cloud Physics

The most immediate implication of our findings is that care must be taken when attempting to use the NGT paleotemperature proxy areas where infiltration into aquifers is too rapid for equilibration to take place at the water table (e.g., fractured aquifer systems). Previous studies (Amalberti et al., 2018; Warrier et al., 2013) had stressed the importance of ice as a starting point for rain formation to explain the widespread findings of He enrichment and heavy noble gas depletion in rainwater and in volcanic island aquifers. However, recent studies from the island of Maui called into question whether precipitation there was likely to have ever been in the form of ice (Niu et al., 2017, 2020). Our present study confirms that liquid cloud water and fog can indeed present similar noble gas signatures as previously seen in northern latitude rain (Warrier et al., 2013) that had likely formed from melted snow or ice.

If our proposed hypothesis suggesting that small liquid water droplets have an ice-like surface of ES water clusters due to buoyancy from the pressure gradient at the surface of the droplet is correct, then the nature of this surface and its stability might account for variations in the so-called accommodation coefficient (α) that different aerosol species display with regard to incorporation within cloud droplets. This purely empirical factor could conceivably be affected by the coherence of an ES-rich surface, in which case large drops that have little surface buoyancy might exhibit a different α than smaller droplets that have a higher surface pressure gradient.

In addition, this hypothesis implies that condensation that causes droplets to grow would energetically favor the arrangement of ES clusters on the surface as opposed to CS clusters. From Equation S19 in Supporting Information S1, one can estimate that the extra potential energy of a CS cluster consisting of 40 molecules at the surface of a 50 nm diameter water droplet at 15°C would be in excess of 800 J per mole of water clusters, or over 20 J per mole of water molecules. The energy cost per mole of water molecules to be in a CS structure on the surface of a 10 nm diameter droplet would exceed 100 J. One can imagine that the droplet surface might always have He excess and heavy noble gas deficiency relative to liquid water and that these characteristics might be transported into the interior of the droplet as it grows due to condensation.

It has not escaped our attention that the hypothesis has further implications for the Kelvin effect that predicts that the vapor pressure near a water droplet will be increased over that for water with a flat surface due to Young-Laplace pressure. The Kelvin equation can be written as:

$$\ln\frac{p}{p_{sat}} = \frac{2\gamma V_m}{rRT}$$

where p is the actual vapor pressure, p_{sat} is the vapor pressure of water if the surface was flat, γ is the surface tension of air/liquid interface, V_m is the molar volume of the liquid, r is the droplet radius, R is the gas constant, and T is the absolute temperature. This equation is in turn a part of Köhler theory that is used to predict the conditions for the growth of cloud condensation nuclei, or CCN (Seinfeld & Pandis, 2016, ch. 17). For pure water, it is assumed that the Kelvin effect totally dominates, which has led to the assumption that extremely small pure water droplets will invariably evaporate due to their elevated vapor pressure. However, as noted by Galvin (2005), the derivation of the Kelvin equation assumes that the liquid is istotropic and homogeneous. If our hypothesis is accurate, however, water droplets, especially those much smaller than 100 μm diameter, will likely have a surface structure very close to that of ice. It is not known at the present time how this might affect the true vapor pressure near cloud water particles, but it is conceivable that the vapor pressure could be much lower than that predicted by the Kelvin equation. This in turn has possible implications for recent hypotheses concerning CCN formation due to cosmic rays (Svensmark et al., 2013, 2016, 2017). Once a pure water droplet has formed, possibly due to nucleation around an ionized atom, the droplet could have a greater than normally anticipated lifetime even without a contaminating aerosol.

5. Conclusions

From the studies by Warrier et al., (2012) and Niu et al., (2017, 2020), it is clear that an understanding of the noble gas concentrations in precipitation is essential for the use of the NGT climate proxy in zones of rapid groundwater recharge, such as is common on volcanic islands. Rain from clouds extending above the freezing layer in the atmosphere was analyzed in Warrier et al. (2013) and snow was examined in Amalberti et al., (2018). In the present study, liquid cloud water samples, including fog-sized droplets, were collected in two mountain sites with distinctly different climates. The noble gas concentration results show similar features to both shallow groundwater (springs) and rain samples in the earlier studies and they resemble partially equilibrated rain from convective clouds extending to altitudes with below-freezing temperatures. Specifically, He is normally in excess and the three heaviest noble gases are significantly depleted with respect to ASW. However, the liquid cloud water samples that were collected were never below the freezing point of water and thus a freeze-melt cycle during the precipitation process is an unlikely explanation for the measured noble gas concentrations.

An extensive set of numerical simulations was performed using the standard model of homogeneous liquid water being formed from melting snow. The model included a range of possible atmospheric lapse rates, temperature and pressure dependent terminal velocities, altitude dependent pressures, temperature dependent noble gas solubilities, and temperature dependent noble gas diffusivities. In all cases, water droplets with a diameter of roughly 1 mm or smaller were nearly completely equilibrated in terms of noble gas concentrations. This result is a conservative estimate because all noble gas transport in cloud water droplets is assumed to be due to diffusion and any advection within the liquid water would be expected to speed up the process of equilibration.

Alternative hypotheses were examined to explain the apparently anomalous results. These included the NP model of Mercury et al., (2003, 2004), wherein positive pressure within the droplets due to surface tension (i.e., Young-Laplace pressure) could reduce the solubility of the noble gases, with the heavy noble gases more affected than the light. However, the NP model requires droplet diameters roughly two to three orders of magnitude smaller than are commonly seen in cloud water. In addition, the NP model cannot account for the He excess that is commonly observed. Although a fortuitous combination of the NP model and excess air (EA) could mimic our results, as soon as the submicron droplets coalesced to the size normally seen in clouds, the high pressures needed to explain the heavy noble gas concentrations would no longer exist. Any such droplet should instantly equilibrate to ASW values.

A novel hypothesis is offered that relies on the hypothesis that liquid water consists of clusters of molecules bound together by hydrogen bonds. This concept of water polymorphism envisions that such clusters exist, and they have a range of densities. For this study, if expanded structure (ES clusters, low density) and condensed structure (CS clusters, high density) coexist within a water droplet, the pressure gradient near the surface of the droplet that is the result of Young-Laplace pressure should provide a buoyancy force that causes CS clusters to "sink" into the interior of a droplet and ES clusters to "float" toward the surface. ES clusters are expected to have a structure similar to that of ice and therefore small water droplets could possibly present a spherical ice-like surface to the surrounding air. In addition, an ice-like surface makes it possible that the Kelvin effect may need to be revisited. A semi-permeable ice-like droplet surface would be compatible with the measured noble gas concentrations in this study.

Simplified estimates of the enthalpy and entropy changes that might result from creation of an ice-like surface are made and it is calculated that the thickness of this layer should be relatively insensitive to droplet diameter. However, the enthalpy reduction from the formation of a surface layer rich in ES clusters is highly dependent on droplet diameter and any solubility effects should rise with decreasing diameter. The results presented here, and the proposed mechanism may have implications for uptake of other nonpolar hydrophobic species in contact with cloud water.

Conflict of Interest

The authors declare no conflicts of interest relevant to this study

Data Availability Statement

Any use of trade, firm, or product names is for descriptive purposes only and does not imply endorsement by the U.S. Government. Supplementary information including software and a detailed data table are archived at doi:10.17632/8xvkmtn58x.1

References

Aeschbach-Hertig, W., Peeters, F., Beyerle, U., & Kipfer, R. (1999). Interpretation of dissolved atmospheric noble gases in natural waters. *Water Resources Research*, *35*(9), 2779–2792.

Aeschbach-Hertig, W., Peeters, F., Beyerle, U., & Kipfer, R. (2000). Palaeotemperature reconstruction from noble gases in ground water taking into account equilibration with entrapped air. *Nature*, *405*(6790), 1040–1044. https://doi.org/10.1038/35016542

Amalberti, J., Hall, C. M., & Castro, M. C. (2018). Noble gas signatures in snow. *Chemical Geology*, *483*, 275–285. https://doi.org/10.1016/j.chemgeo.2018.02.022

Ball, P. (2008). Water—An enduring mystery. *Nature*, *452*(7185), 291–292. https://doi.org/10.1038/452291a

Ballentine, C. J., & Hall, C. M. (1999). Determining paleotemperature and other variables using noble gas concentrations in water. *Geochimica et Cosmochimica Acta*, *63*, 2315-2336. https://doi.org/10.1016/s0016-7037(99)00131-3

Bassiouni, M., Scholl, M. A., Torres-Sanchez, A. J., & Murphy, S. F. (2017). A method for quantifying cloud immersion in a tropical mountain forest using time-lapse photography. *Agricultural and Forest Meteorology*, *243*, 100–112. https://doi.org/10.1016/j.agrformet.2017.04.010

Bergquist, B. A., & Blum, J. D. (2009). The odds and evens of mercury isotopes: Applications of mass-dependent and mass-independent isotope fractionation. *Elements*, *5*(6), 353–357. https://doi.org/10.2113/gselements.5.6.353

Berry, Z. C., Hughes, N. M., & Smith, W. K. (2014). Cloud immersion: An important water source for spruce and fir saplings in the southern Appalachian Mountains. *Oecologia*, *174*, 319–326. https://doi.org/10.1007/s00442-013-2770-0

Best, A. C. (1950). Empirical formulae for the terminal velocity of water drops falling through the atmosphere. *Quarterly Journal of the Royal Meteorological Society*, *76*(329), 302–311. https://doi.org/10.1002/qj.49707632905

Buck, U., Pradzynski, C. C., Zeuch, T., Dieterich, J. M., & Hartke, B. (2014). A size resolved investigation of large water clusters. *Physical Chemistry Chemical Physics*, *16*(15), 6859–6871. https://doi.org/10.1039/c3cp55185g

Castro, M. C., Hall, C. M., Patriarche, D., Goblet, P., & Ellis, B. R. (2007). A new noble gas paleoclimate record in Texas—Basic assumptions revisited. *Earth and Planetary Science Letters*, *257*(1–2), 170–187. https://doi.org/10.1016/j.epsl.2007.02.030

Chaplin, M. F. (2000). A proposal for the structuring of water. *Biophysical Chemistry*, *83*(3), 211–221. https://doi.org/10.1016/s0301-4622(99)00142-8

Daube, B. C., Jr, Flagan, R. C., & Hoffmann, M. R. (1987). *Active cloudwater collector*. (p. 462). United States Patent No, 4697.

De Gennes, P. G., Brochard-Wyart, F., & Quéré, D. (2013). *Capillarity and wetting phenomena: Drops, bubbles, pearls, waves*. Springer Science & Business Media.

Demoz, B. B., Collett, J. L., Jr, & Daube, B. C., Jr (1996). On the caltech active strand cloudwater collectors. *Atmospheric Research*, *41*, 47–62. https://doi.org/10.1016/0169-8095(95)00044-5

Douillard, J. M. (2009). Experimental approach of the relation between surface tension and interfacial thickness of simple liquids. *Journal of Colloid and Interface Science*, *337*, 307–310. https://doi.org/10.1016/j.jcis.2009.04.084

Elperin, T., Fominykh, A., & Krasovitov, B. (2009). Effect of altitude concentration gradient of soluble gaseous pollutants on their scavenging by falling rain droplets. *Journal of the Atmospheric Sciences*, *66*, 2349–2358. https://doi.org/10.1175/2009jas2922.1

Ervens, B., Sorooshian, A., Aldhaif, A. M., Shingler, T., Crosbie, E., Ziemba, L., et al. (2018). Is there an aerosol signature of chemical cloud processing? *Atmospheric Chemistry and Physics*, *18*, 16099–16119. https://doi.org/10.5194/acp-18-16099-2018

Eugster, W., Burkard, R., Holwerda, F., Scatena, F. N., & Bruijnzeel, L. A. (2006). Characteristics of fog and fogwater fluxes in a Puerto Rican elfin cloud forest. *Agricultural and Forest Meteorology*, *139*, 288–306. https://doi.org/10.1016/j.agrformet.2006.07.008

Foote, G. B., & Du Toit, P. S. (1969). Terminal velocity of raindrops aloft. *Journal of Applied Meteorology*, *8*(2), 249–253. https://doi.org/10.1175/1520-0450(1969)008<0249:tvora>2.0.co;2

Füri, E., Hilton, D. R., Brown, K. M., & Tryon, M. D. (2009). Helium systematics of cold seep fluids at Monterey Bay, California, USA: Temporal variations and mantle contributions. *Geochemistry, Geophysics, Geosystems*, *10*(8).

Gallo, P., Amann-Winkel, K., Angell, C. A., Anisimov, M. A., Caupin, F., Chakravarty, C., et al. (2016). Water: A tale of two liquids. *Chemical Reviews*, *116*(13), 7463–7500. https://doi.org/10.1021/acs.chemrev.5b00750

Galvin, K. P. (2005). A conceptually simple derivation of the Kelvin equation. *Chemical Engineering Science*, *60*(16), 4659–4660. https://doi.org/10.1016/j.ces.2005.03.030

Garcia-Ratés, M., Miró, P., Poblet, J. M., Bo, C., & Avalos, J. B. (2011). Dynamics of encapsulated water inside Mo132 cavities. *The Journal of Physical Chemistry B*, *115*(19), 5980–5992.

Gioda, A., Mayol-Bracero, O. L., Scatena, F. N., Weathers, K. C., Mateus, V. L., & McDowell, W. H. (2013). Chemical constituents in clouds and rainwater in the Puerto Rican rainforest: Potential sources and seasonal drivers. *Atmospheric Environment*, *68*, 208–220. https://doi.org/10.1016/j.atmosenv.2012.11.017

Gultepe, I., Tardif, R., Michaelides, S. C., Cermak, J., Bott, A., Bendix, J., et al. (2007). Fog research: A review of past achievements and future perspectives. *Pure and Applied Geophysics*, *164*(6–7), 1121–1159. https://doi.org/10.1007/978-3-7643-8419-7_3

Hall, C. M., Castro, M. C., Lohmann, K. C., & Sun, T. (2012). Testing the noble gas paleothermometer with a yearlong study of groundwater noble gases in an instrumented monitoring well. *Water Resources Research*, *48*, W04517. https://doi.org/10.1029/2011WR010951

Heaton, T. H. E., & Vogel, J. C. (1981). Excess air in groundwater. *Journal of Hydrology*, *50*, 201–216. https://doi.org/10.1016/0022-1694(81)90070-6

Holz, M., Haselmeier, R., Mazitov, R. K., & Weingaertner, H. (1994). Self-diffusion of neon in water by ^{21}Ne NMR. *Journal of the American Chemical Society*, *116*(2), 801–802. https://doi.org/10.1021/ja00081a064

Huang, Y., Zhang, X., Ma, Z., Li, W., Zhou, Y., Zhou, J., et al. (2013). Size, separation, structural order, and mass density of molecules packing in water and ice. *Scientific Reports*, *3*, 3005. https://doi.org/10.1038/srep03005

Huber, C., Beyerle, U., Leuenberger, M., Schwander, J., Kipfer, R., Spahni, R., et al. (2006). Evidence for molecular size dependent gas fractionation in firn air derived from noble gases, oxygen, and nitrogen measurements. *Earth and Planetary Science Letters*, *243*(1), 61–73. https://doi.org/10.1016/j.epsl.2005.12.036

Jähne, B., Heinz, G., & Dietrich, W. (1987). Measurement of the diffusion coefficient of sparingly soluble gases in water. *Journal of Geophysical Research*, *92*, 10767–10776.

Kipfer, R., Aeschbach-Hertig, W., Peeters, F., & Stute, M. (2002). Noble gases in lakes and ground waters. *Reviews in Mineralogy and Geochemistry*, *47*(1), 615–700. https://doi.org/10.2138/rmg.2002.47.14

Li, Z., & Aneja, V. P. (1992). Regional analysis of cloud chemistry at high elevations in the eastern United States. *Atmospheric Environment Part A. General Topics*, *26*(11), 2001–2017. https://doi.org/10.1016/0960-1686(92)90085-y

Malone, J. L., Castro, M. C., Hall, C. M., Doran, P. T., Kenig, F., & McKay, C. P. (2010). New insights into the origin and evolution of Lake Vida, McMurdo Dry Valleys, Antarctica—A noble gas study in ice and brines. *Earth and Planetary Science Letters*, *289*(1), 112–122. https://doi.org/10.1016/j.epsl.2009.10.034

Manning, A. H., & Solomon, D. K. (2003). Using noble gases to investigate mountain-front recharge. *Journal of Hydrology*, *275*(3–4), 194–207. https://doi.org/10.1016/s0022-1694(03)00043-x

Mazor, E. (1972). Paleotemperatures and other hydrological parameters deduced from noble gases dissolved in groundwaters; Jordan Rift Valley, Israel. *Geochimica et Cosmochimica Acta*, *36*(12), 1321–1336. https://doi.org/10.1016/0016-7037(72)90065-8

Mercury, L., Mohamed, A., Hermann, Z., & Tardy, Y. (2003). Thermodynamic properties of solutions in metastable systems under negative or positive pressures. *Geochimica et Cosmochimica Acta*, *67*(10), 1769–1785. https://doi.org/10.1016/S0016-7037(02)01406-0

Mercury, L., Pinti, D. L., & Zeyen, H. (2004). The effect of the negative pressure of capillary water on atmospheric noble gas solubility in ground water and palaeotemperature reconstruction. *Earth and Planetary Science Letters*, *223*(1–2), 147–161. https://doi.org/10.1016/j.epsl.2004.04.019

Mishima, O., & Stanley, H. E. (1998). The relationship between liquid, supercooled and glassy water. *Nature*, *396*(6709), 329–335. https://doi.org/10.1038/24540

Müller, A., Bögge, H., & Diemann, E. (2003). Structure of a cavity-encapsulated nanodrop of water. *Inorganic Chemistry Communications*, *3*(6), 52329.

Niu, Y., Castro, M. C., Hall, C. M., Gingerich, S. B., Scholl, M. A., & Warrier, R. B. (2017). Noble gas signatures in the Island of Maui, Hawaii: Characterizing groundwater sources in fractured systems. *Water Resources Research*, *53*(5), 3599–3614. https://doi.org/10.1002/2016wr020172

Niu, Y., Castro, M. C., Hall, C. M., Poulsen, C. J., Lohmann, K. C., & Aron, P. (2020). Groundwater sources in the Island of Maui, Hawaii—A combined noble gas, stable isotope, and tritium approach. *Applied Geochemistry*, *117*, 104587. https://doi.org/10.1016/j.apgeochem.2020.104587

Ozima, M., & Podosek, F. A. (2002). *Noble gas geochemistry*. Cambridge University Press.

Pye, H. O. T., Nenes, A., Alexander, B., Ault, A. P., Barth, M. C., Clegg, S. L., et al. (2020). The acidity of atmospheric particles and clouds. *Atmospheric Chemistry and Physics*, *20*, 4809–4888. https://doi.org/10.5194/acp-20-4809-2020

Scholl, M. A., Gingerich, S. B., & Tribble, G. W. (2002). The influence of microclimates and fog on stable isotope signatures used in interpretation of regional hydrology: East Maui, Hawaii. *Journal of Hydrology*, *264*, 170–184. https://doi.org/10.1016/s0022-1694(02)00073-2

Seinfeld, J. H., & Pandis, S. N. (2016). *Atmospheric chemistry and physics: From air pollution to climate change*. John Wiley & Sons.

Seltzer, A. M., Ng, J., & Severinghaus, J. P. (2019). Precise determination of Ar, Kr and Xe isotopic fractionation due to diffusion and dissolution in fresh water. *Earth and Planetary Science Letters*, *514*, 156–165. https://doi.org/10.1016/j.epsl.2019.03.008

Spiegel, J. K., Buchmann, N., Mayol-Bracero, O. L., Cuadra-Rodriguez, L. A., Díaz, C. J. V., Prather, K. A., et al. (2014). Do cloud properties in a Puerto Rican tropical montane cloud forest depend on occurrence of long-range transported African dust? *Pure and Applied Geophysics*, *171*(9), 2443–2459. https://doi.org/10.1007/s00024-014-0830-y

Stute, M., & Schlosser, P. (1993). Principles and applications of the noble gas paleothermometer. *Climate Change in Continental Isotopic Records*, *78*, 89–100.

Stute, M., Schlosser, P., Clark, J. F., & Broecker, W. S. (1992). Paleotemperatures in the Southwestern United States derived from noble gases in ground water. *Science*, *256*(5059), 1000–1003. https://doi.org/10.1126/science.256.5059.1000

Sun, T., Hall, C. M., & Castro, M. C. (2010). Statistical properties of groundwater noble gas paleoclimate models: Are they robust and unbiased estimators? *Geochemistry, Geophysics, Geosystems*, *11*(2). https://doi.org/10.1029/2009gc002717

Svensmark, H., Enghoff, M. B., & Pedersen, J. O. P. (2013). Response of cloud condensation nuclei (> 50 nm) to changes in ion-nucleation. *Physics Letters A*, *377*(37), 2343–2347. https://doi.org/10.1016/j.physleta.2013.07.004

Svensmark, H., Enghoff, M. B., Shaviv, N. J., & Svensmark, J. (2017). Increased ionization supports growth of aerosols into cloud condensation nuclei. *Nature Communications*, *8*(1), 1–9. https://doi.org/10.1038/s41467-017-02082-2

Svensmark, J., Enghoff, M. B., Shaviv, N. J., & Svensmark, H. (2016). The response of clouds and aerosols to cosmic ray decreases. *Journal of Geophysical Research: Space Physics*, *121*(9), 8152–8181. https://doi.org/10.1002/2016ja022689

Tarasevich, Y. I. (2011). State and structure of water in vicinity of hydrophobic surfaces. *Colloid Journal*, *73*(2), 257–266. https://doi.org/10.1134/s1061933x11020141

Top, Z., Martin, S., & Becker, P. (1988). A laboratory study of dissolved noble gas anomaly due to ice formation. *Geophysical Research Letters*, *15*(8), 796–799. https://doi.org/10.1029/gl015i008p00796

Utting, N., Lauriol, B., Lacelle, D., & Clark, I. (2016). Using noble gas ratios to determine the origin of ground ice. *Quaternary Research*, *85*(1), 177–184. https://doi.org/10.1016/j.yqres.2015.12.003

Vedamuthu, M., Singh, S., & Robinson, G. W. (1994). Properties of liquid water: Origin of the density anomalies. *The Journal of Physical Chemistry*, *98*(9), 2222–2230. https://doi.org/10.1021/j100060a002

Wallace, J. M., & Hobbs, P. V. (2006). *Atmospheric science: An introductory survey* (92). Elsevier Academic Press.

Warrier, R. B., Castro, M. C., & Hall, C. M. (2012). Recharge and source-water insights from the Galapagos islands using noble gases and stable isotopes. *Water Resources Research*, *48*, W03508. https://doi.org/10.1029/2011WR010954

Warrier, R. B., Clara Castro, M., Hall, C. M., & Lohmann, K. C. (2013). Noble gas composition in rainwater and associated weather patterns, *Geophysical Research Letters*, *40*, 3248–3252. https://doi.org/10.1002/grl.50610

Weathers, K. C., Simkin, S. M., Lovett, G. M., & Lindberg, S. E. (2006). Empirical modeling of atmospheric deposition in mountainous landscapes. *Ecological Applications*, *16*(4), 1590–1607. https://doi.org/10.1890/1051-0761(2006)016[1590:emoadi]2.0.co;2

Weiss, R. F. (1968). Piggyback sampler for dissolved gas studies on sealed water samples. *Deep Sea Research and Oceanographic Abstracts*, *15*, 695–699. https://doi.org/10.1016/0011-7471(68)90082-x

References From the Supporting Information

Crank, J. (1979). *The mathematics of diffusion*. Oxford University Press.

Roos, N. (2014). Entropic forces in Brownian motion. *American Journal of Physics*, *82*(12), 1161–1166.